



HAL
open science

Partial re-investigation of the ternary diagram $\text{La}_2\text{O}_3 - \text{Nb}_2\text{O}_5 - \text{CaO}$, synthesis and characterization of the $\text{Ca}_2\text{La}_3\text{Nb}_3\text{O}_{14}$ and $\text{Ca}_8\text{La}_8\text{Nb}_{14.4} 1.6\text{O}_{56}$ compounds

Q Ye, Alain Jouanneaux, Emmanuelle Suard, François Goutenoire

► To cite this version:

Q Ye, Alain Jouanneaux, Emmanuelle Suard, François Goutenoire. Partial re-investigation of the ternary diagram $\text{La}_2\text{O}_3 - \text{Nb}_2\text{O}_5 - \text{CaO}$, synthesis and characterization of the $\text{Ca}_2\text{La}_3\text{Nb}_3\text{O}_{14}$ and $\text{Ca}_8\text{La}_8\text{Nb}_{14.4} 1.6\text{O}_{56}$ compounds. *Journal of Solid State Chemistry*, 2022, 314, pp.123390. 10.1016/j.jssc.2022.123390 . hal-03723231

HAL Id: hal-03723231

<https://hal.science/hal-03723231>

Submitted on 20 Jul 2022

HAL is a multi-disciplinary open access archive for the deposit and dissemination of scientific research documents, whether they are published or not. The documents may come from teaching and research institutions in France or abroad, or from public or private research centers.

L'archive ouverte pluridisciplinaire **HAL**, est destinée au dépôt et à la diffusion de documents scientifiques de niveau recherche, publiés ou non, émanant des établissements d'enseignement et de recherche français ou étrangers, des laboratoires publics ou privés.

Partial re-investigation of the ternary diagram La_2O_3 - Nb_2O_5 - CaO , synthesis and characterization of the $\text{Ca}_2\text{La}_3\text{Nb}_3\text{O}_{14}$ and $\text{Ca}_8\text{La}_8\text{Nb}_{14.4}\square_{1.6}\text{O}_{56}$ compounds.

Q. Ye^a, A. Jouanneaux^a, E. Suard^b and F. Goutenoire^a

^a IMMM (Institut des Molécules et Matériaux du Mans), UMR-CNRS 6283, Le Mans Université, 72085 Le Mans Cedex 9, France.

^b ILL (Institut Laue Langevin), Avenue des Martyrs, B. P. 156, 38042 Grenoble Cedex, France.

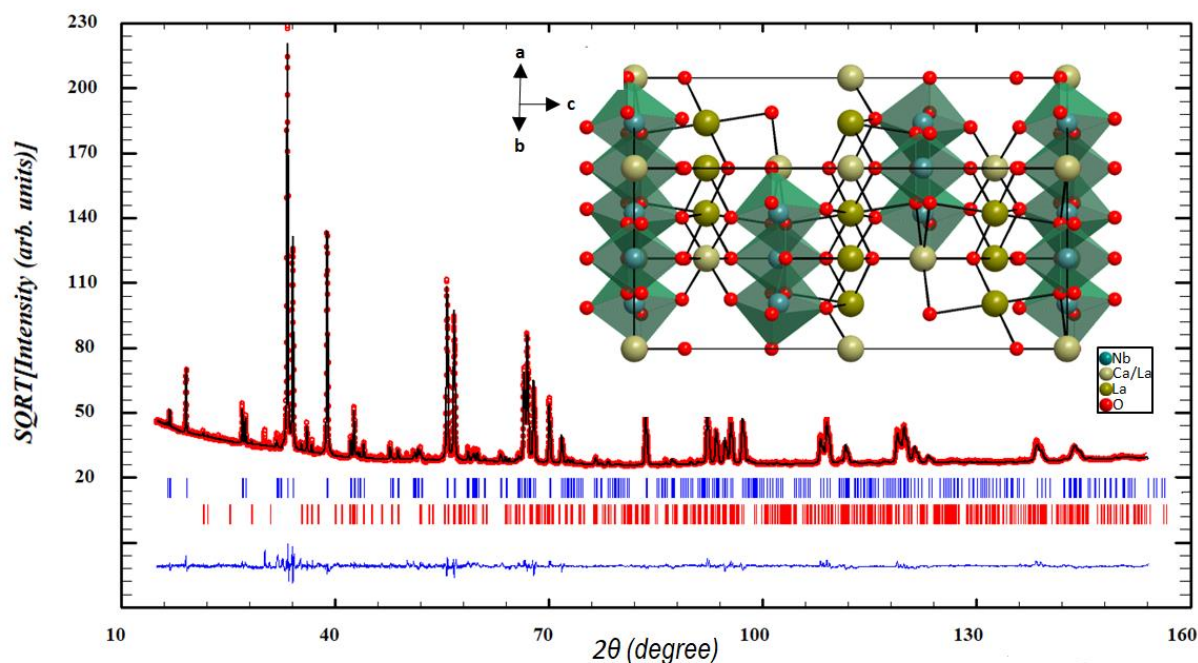
Abstract

This paper focuses on the synthesis and the structure determination of two previously reported compounds of unknown structure - $\text{Ca}_{0.96}\text{La}_{1.56}\text{Nb}_{1.48}\text{O}_7$ and $\text{Ca}_{1.16}\text{La}_{1.26}\text{Nb}_{1.56}\text{O}_7$ - as well as the investigation of the center of the ternary phases diagram La_2O_3 - Nb_2O_5 - CaO . The samples are prepared by the conventional solid state ceramic route. Structure determination is performed by using microscopy electron diffraction, X-ray and neutron powder diffraction data. The formulas of the two compounds are found to be $\text{Ca}_2\text{La}_3\text{Nb}_3\text{O}_{14}$ and $\text{Ca}_8\text{La}_8\text{Nb}_{14.4}\square_{1.6}\text{O}_{56}$, respectively, where the symbol \square denotes cationic vacancies. $\text{Ca}_2\text{La}_3\text{Nb}_3\text{O}_{14}$ crystallizes in the rhombohedral space group $R\bar{3}m$ (No.166) ($Z = 3$) with the cell parameters $a = 7.6525(2)$ (Å) and $c = 18.2981(5)$ (Å). $\text{Ca}_8\text{La}_8\text{Nb}_{14.4}\square_{1.6}\text{O}_{56}$ crystallizes in the cubic space group $Fd\bar{3}m$ (No.227) ($a = 10.6111(1)$ (Å), $Z = 1$). In both structures, Calcium and Lanthanum atoms are randomly distributed on the appropriate crystallographic sites. Both compounds belong to the Pyrochlore family $A_2B_2X_7$. Their conduction properties are studied with complex impedance spectroscopy.

The central region of the ternary diagram La_2O_3 - Nb_2O_5 - CaO , investigated using Rietveld refinements on X-ray diffraction data, is found to be composed of 8 zones which are in agreement with Gibbs rules from a thermodynamic point of view.

Graphical abstract

In the ternary phase diagram $\text{La}_2\text{O}_3 - \text{Nb}_2\text{O}_5 - \text{CaO}$, a new rhombohedral Pyrochlore and a new cubic Pyrochlore are discovered. The study of their structures and of their transport properties is reported in this paper.



Keywords

Fuel Cells, Electrolyte materials, Crystal structure determination, Rietveld refinement, Solid solution, Ionic conduction.

1. Introduction

Fuel Cells (FCs) are electrochemical devices that enable direct conversion of the chemical energy of fuels into electricity. They are one of the most promising alternatives to traditional power generation technologies in order to achieve low-carbon transformation. FCs use hydrogen, methane, and methanol, etc. as fuels, which enables pollutant emissions to be reduced as compared with the use of fossil energy. FCs can even reduce pollutant emission to zero when using hydrogen as fuel ^[1]. On the other hand, FCs convert chemical energy directly into electrical energy, which enables energy conversion loss to be minimized to get higher energy conversion efficiency. This feature is a huge advantage as compared with traditional mechanical equipment using indirect conversion (chemical energy → thermal energy → mechanical energy → electrical energy). Actually, the voltage efficiencies at typical operating current density of different types of FCs are generally in the range of 50% to 60% ^[1]. Among FCs, Solid Oxide Fuel Cells (SOFCs) are the most competitive; their electrical

power generation efficiencies are typically in the range from 60% to 65%, with the highest reaching more than 80% in the case of cogeneration ^[1]. It can be noticed that the weighted average efficiencies are 35% for coal, 45% for natural gas and 38% for oil fired power generation by the traditional power generation technologies ^[2].

The SOFCs use solid ceramic electrolytes which are more sturdy, more reliable, more secure and easier to mould than liquid electrolytes. The most popular solid electrolyte materials are Zirconia-based oxide ion conductors: Yttria-stabilized Zirconia (YSZ) ^{[3][4][5]}. Other potential electrolyte materials include Ceria-based oxide ion conductors ^{[6][7]}, Perovskite-structured oxide ion conductors with the general formula ABO_3 ^{[6][8][10]}, Brownmillerite-structured oxide ion conductors ($A_2B'B''O_5$ or $A_2B_2O_5$) ^{[9][10]}, LAMOX family ($La_2Mo_2O_9$ and the derivatives) ^{[11][12][13]} and proton conducting oxides which transport hydrogen ions instead of oxygen ions. The main advantage of proton conductors is that the FCs do not require water removing unit because proton conductors generate steam in oxidant electrode (cathode) ^{[6][14]}. However, all these electrolyte materials operate only in high temperature range (800°C - 1000°C), which leads to a series of significant technical challenges, such as the development of compatible materials, the improvement of the service life, the reduction of the production costs and so on. Consequently, seeking electrolyte materials that can operate at medium and low temperatures is the key objectives of the research work on SOFCs.

In recent years, the transport properties of the phases La_3NbO_7 , $LaNb_3O_9$, $LaNbO_4$ located in the binary phase diagram $La_2O_3 - Nb_2O_5$ as well as of their derivatives were widely studied. La_3NbO_7 has an orthorhombic Weberite-type crystal structure and undergoes a phase transition at about 360K due to a slight change in symmetry. Below 360K, La_3NbO_7 crystallizes in the space group $Pm\bar{c}n$ (No.62) while its structure is described in the space group $Cmcm$ (No.63) above the phase transition temperature ^{[15][16]}. La_3NbO_7 typically behaves as a pure oxide-ion conductor with a stable conductivity level over a wide range of oxygen partial pressure. Nevertheless, its conductivity is relatively low due to the lack of oxygen vacancies. The transport properties of its derivatives can be improved by doping with lower valence ions (e.g. Ca^{2+} , Sr^{2+} , Ba^{2+}) ^{[17][18][19][20]}. Similarly, $LaNb_3O_9$ exhibits a reversible phase transition between the low temperature α -polymorph (orthorhombic) and the high temperature β -polymorph (tetragonal), the latter being a A(site)-cation-deficient Perovskite above about 195°C ^[21]. β - $LaNb_3O_9$ which displays a mixed ionic-electronic conduction has been reported by A.M. George and A.N. Virkar ^[22]. Regarding $LaNbO_4$, its room temperature phase crystallizes in the monoclinic Scheelite structure with space group $I2/a$ (No.15) while the material crystallizes in the tetragonal system with space group $I4_1/a$ (No.88) at high temperature. The reversible phase transition occurs around 530°C ^[23]. $LaNbO_4$ and its acceptor-doped derivatives display proton conduction properties. The maximum proton conductivity reaches the order of 10^{-3} S/cm in atmosphere of 2.5% H_2O at 950°C for 1% Ca-doped $LaNbO_4$. Moreover, this derivative $La_{0.99}Ca_{0.01}NbO_4$ shows high chemical

stability in humid and CO₂-containing environment [24][25][26][27]. This result is in good agreement with theoretical predictions which indicated that partial substitution of higher valence Lanthanum ions (+3) and/or Niobium ions (+5) with lower valence ions (e.g. Ca²⁺) possibly generates more stable and more conductive new phases with defective structures. The high conductivity of La_{0.99}Ca_{0.01}NbO₄ also aroused our interest in the ternary phase diagram La₂O₃ - Nb₂O₅ - CaO previously studied by A.M. Frolov and A.A. Evdokimov [28], in which we noticed that two phases with the following formulas: Ca_{0.96}La_{1.56}Nb_{1.48}O₇ and Ca_{1.16}La_{1.26}Nb_{1.56}O₇ were not structurally characterized (**Figure 1**). PDF files are available with the references 00-040-0438 and 00-048-0419 for respectively the first compound having a rhombohedral cell with a = 7.655 Å and c = 18.31 Å, and the second one having a cubic cell with a = 10.504 Å.

This work addresses the synthesis, the crystal structure determination and the measurement of the ionic conductivity of both compounds. A partial re-investigation of the central region of the ternary phase diagram La₂O₃ - Nb₂O₅ - CaO from a thermodynamic point of view is also carried out.

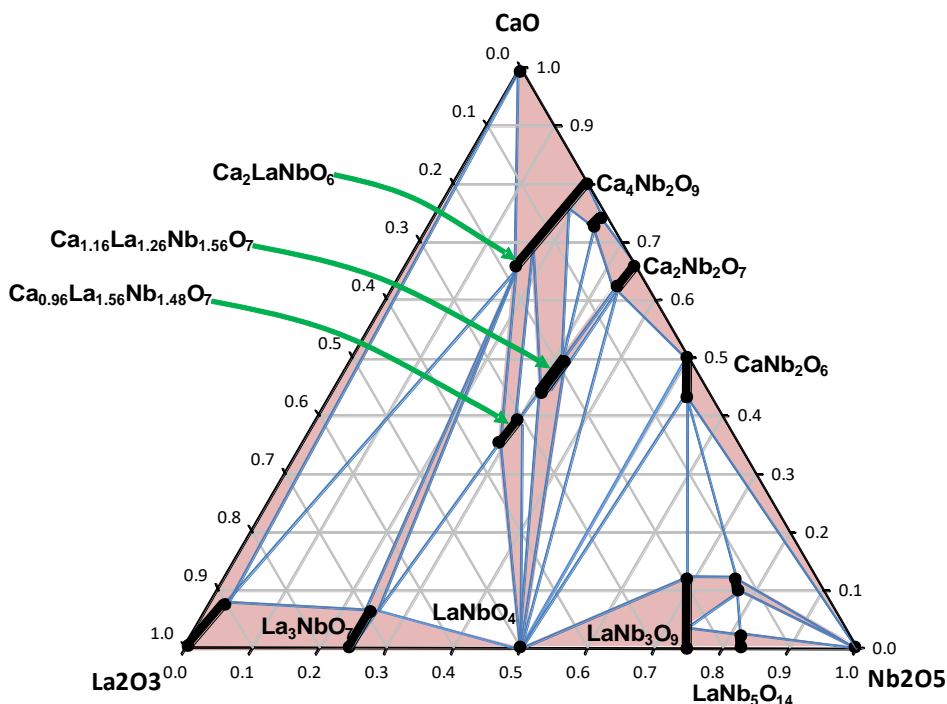


Figure 1: Phase diagram La₂O₃-Nb₂O₅-CaO at 1280°C, redrawn from the work of Frolov and Evdokimov [28]. The solid solution areas are marked with bold black lines. The two phase areas are colored in pale pink.

2. Exploring the ternary diagram

As a strategy of this work, a skeleton of 36 compositions was defined in the ternary diagram as shown in the **Figure 2**. They are labeled using alphabetic order from A to Z and then from AA to AJ. In order to investigate more closely the center of the phase diagram, additional compositions were

defined around the X point of nominal composition: 30%Nb₂O₅, 40%CaO and 30%La₂O₃, as shown in the inset in **Figure 2**. At last, a total of 30 compositions were synthesized as illustrated in **Figure 3**.

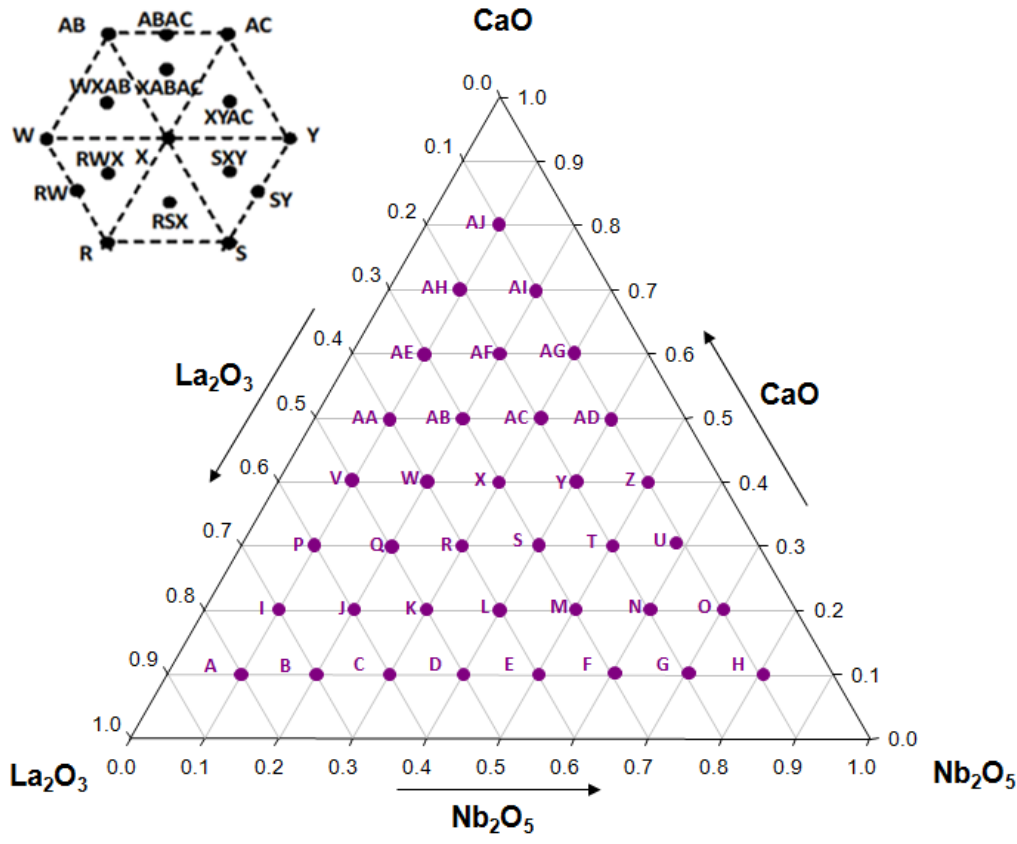


Figure 2: Skeleton of the labeled points from A to Z and AA to AJ. The inset is a zoom around the X point showing the labeling of the additional points.

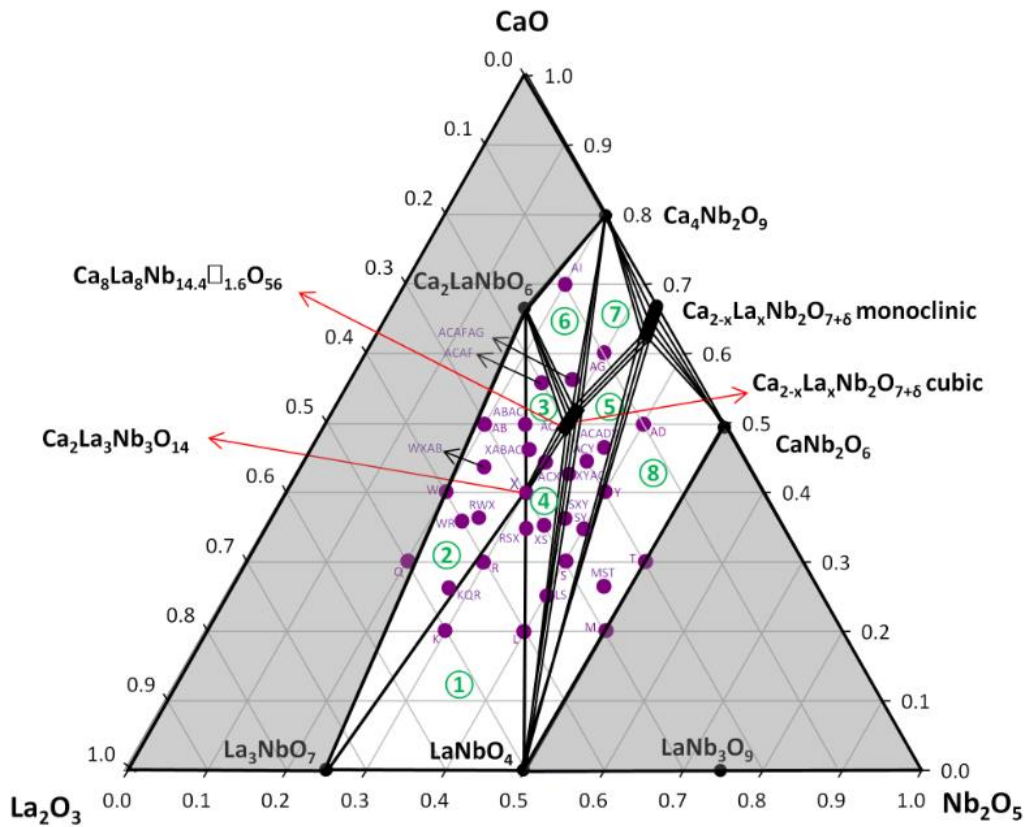


Figure 3: The ternary phase diagram showing the 30 synthesized compositions together with the 8 identified zones as described in the section 8.

3. Experiments

3.1 Synthesis

The compounds were prepared from La_2O_3 , CaCO_3 and Nb_2O_5 . Prior to use, the lanthanum oxide was heated over a night at 1000°C . The different starting materials were weighted in stoichiometric proportion and ground together in an agate mortar and the final mixed powder was placed in alumina crucible. In order to prepare a quasi-pure compound of a large amount of 15g, the powder was annealed at high temperatures according to the process reported in **Table 1** with heating and cooling rates of $6^\circ\text{C}/\text{min}$.

Anneal	Temperature ($^\circ\text{C}$)	Duration (h)
1 st	1300	60
2 nd	1400	60
3 rd	1400	240

Table 1: Temperature and duration of annealing procedure.

3.2 Material characterization using diffraction

The room temperature powder X-ray diffraction (XRD) patterns were collected on a PANalytical-Malvern MPD in Bragg-Brentano geometry equipped with a cobalt X-ray tube. Experimental

conditions for XRD data collection are gathered in **Table 2** for the studied compounds. For the $\text{Ca}_2\text{La}_3\text{Nb}_3\text{O}_{14}$ compound a special variable-counting-time (VCT) procedure was applied ^[29] as described in **Table 3**.

Compound	2 θ -range (°)	Total duration
$\text{Ca}_2\text{La}_3\text{Nb}_3\text{O}_{14}$ rhombohedral	10 - 157	39 h
$\text{Ca}_{2-x}\text{La}_x\text{Nb}_2\text{O}_{7+\delta}$ monoclinic	10 - 120	5 h
$\text{Ca}_8\text{La}_8\text{Nb}_{14.4}\square_{1.6}\text{O}_{56}$ cubic	16 - 156	70 h

Table 2: Experimental conditions for powder XRD data collection.

Scan	Range (°)	Step (°)	Time/Step (s)	Total time / scan	Cycles	Total time
VCT1	10-60	0.017	210	1h 26min	×2	2h 52min
VCT2	59-110	0.017	210	1h 27min	×8	11h 36min
VCT3	109-157	0.017	210	1h 22min	×18	24h 36min

Table 3: Details of the Variable-Counting Time (VCT) strategy for $\text{Ca}_2\text{La}_3\text{Nb}_3\text{O}_{14}$.

Thermal XRD patterns were also acquired from 50°C to 1050°C for both $\text{Ca}_2\text{La}_3\text{Nb}_3\text{O}_{14}$ and $\text{Ca}_8\text{La}_8\text{Nb}_{14.4}\square_{1.6}\text{O}_{56}$ with the diffractometer equipped an Anton Paar HTK12 furnace.

The neutron powder diffraction patterns of both compounds were collected at room temperature on the D2B Debye-Scherrer diffractometer at ILL, Grenoble, France in the 2 θ -range from 5 to 159° at $\lambda \approx 1.594 \text{ \AA}$ with a step of 0.05°(2 θ). The duration of the data collection is about 2 h.

The transmission electron microscopy (TEM) JEOL STEM 2100 with a double-tilt specimen holder was used for electron diffraction investigation at 200kV and room temperature. For the sample preparation, a small amount of sample powder was slightly ground in a mortar and then mixed with ethanol. A drop of this mixture was deposited on the carbon surface of a 1000 mesh copper grid and dried.

3.3 Electrochemical measurement

The transport properties of the compounds were studied by complex impedance spectroscopy in the frequency range from 1M Hz to 1 Hz with alternative voltage of 1V amplitude, by using a Schlumberger Solartron SI 1260 frequency response analyzer connected to a Solartron 1296 dielectric interface with smart impedance software for data collection in dry air and humid air atmosphere. Eight millimeters diameter pellets with, as electrodes, a thin platinum layer deposited on both faces were used for the measurements.

4. Structure investigation of $\text{Ca}_2\text{La}_3\text{Nb}_3\text{O}_{14}$

4.1 Indexation, formulation and space group determination

After a careful analysis of the different patterns for all studied compositions, we can conclude that a new phase is observed around the nominal composition: 30% Nb_2O_5 , 40% CaO and 30% La_2O_3 corresponding to the X point in **Figure 2**. The first crystallographic analysis was performed via a combination of electronic diffraction and auto-indexation procedure using XRD data. The auto-indexation program Treor^[30] implemented in the HighScorePlus program^[31] yields a solution in the hexagonal system with $a = 7.6337 \text{ \AA}$, $c = 18.276 \text{ \AA}$ and $V \approx 922 \text{ \AA}^3$ with $F_{20} = 44$ ^[32]. From the observed and calculated electronic diffraction patterns, a rhombohedral cell clearly appears with the parameters $a \approx 7.6 \text{ \AA}$ and $c \approx 18.3 \text{ \AA}$ (**Figure 4**). The electron diffraction patterns were calculated using CrysTBox^[33].

The general formulation of the new compound and the number of chemical units per unit cell (Z) were extrapolated using i) the average volume of oxygen (in the range $18 - 22 \text{ \AA}^3$) observed in oxides combined with ii) the nominal composition:

- i) The maximum and minimum numbers of oxygen per cell can be calculated from both the cell volume and the maximum and minimum average volume of oxygen respectively:

$$\text{Maximum number} = 922/18 \approx 51$$

$$\text{Minimum number} = 922/22 \approx 42$$

- ii) The nominal composition 40% CaO - 30% La_2O_3 - 30% Nb_2O_5 leads to an initial formula



The appropriate number of oxygen per cell is easily obtained from $\text{Ca}_4\text{La}_6\text{Nb}_6\text{O}_{28} \times 3/2$ leading to the following solution for the chemical composition: $\text{Ca}_2\text{La}_3\text{Nb}_3\text{O}_{14}$ with $Z = 3$.

In order to determine the space group of this compound, the Le Bail refinement procedure^[34] was launched on XRD pattern in space group $R\bar{3}m$ (No.160) using the Fullprof program^[35]. A careful examination of the diffraction pattern shows the presence of Bragg peaks with the indexations (003) and (009) which do not satisfy the reflection condition: $00l$ with $l = 6n$. As a conclusion, five space groups could be used: $R3$ (No.146), $R\bar{3}$ (No.148), $R32$ (No.155), $R3m$ (No.160) and $R\bar{3}m$ (No.166).

By querying in the Inorganic Crystal Structure Database (ICSD) with both the parameters ANX: $\text{A}_2\text{B}_3\text{C}_3\text{X}_{14}$ and the trigonal symmetry, a family of 18 isotype compounds is obtained (**Table 4**), whose general formula is $\text{A}_2\text{Ln}_3\text{Sb}_3\text{O}_{14}$ with ($A = \text{Mg, Ca, Mn and Co}$) and ($\text{Ln} = \text{La, Pr, Sm, Gd}$)^{[36][37][38]}. The structure of all of them is described in the space group $R\bar{3}m$ (N°166).

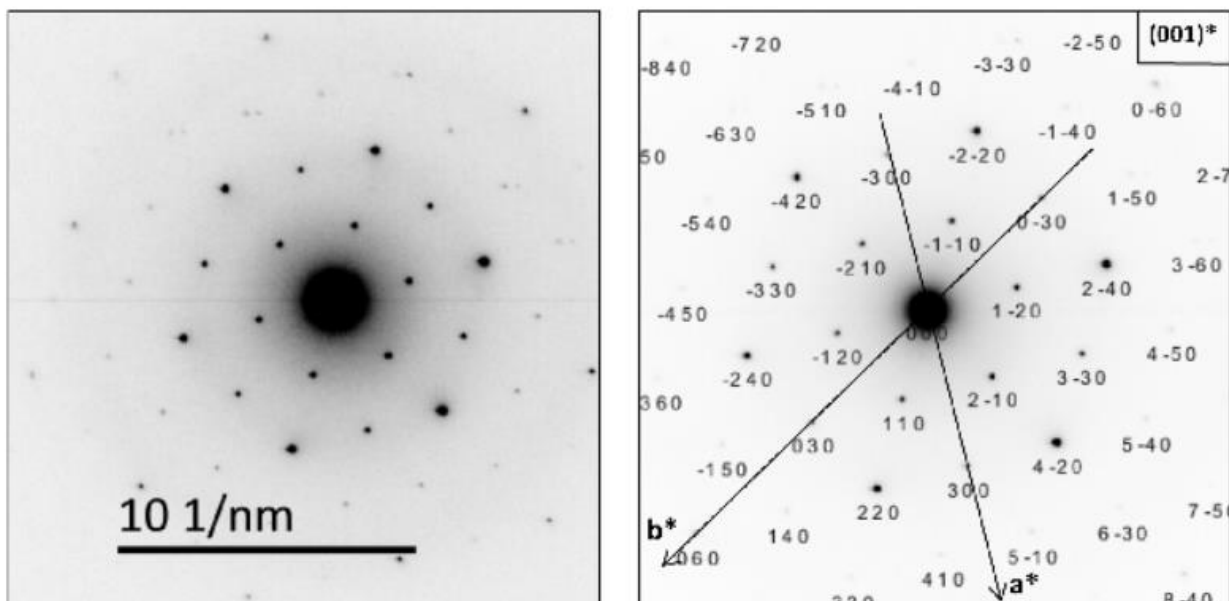


Figure 4: Electron diffraction pattern along (001)* direction plus the indexation from CrystBox program.

Name	a (Å)	c (Å)	V (Å ³)	Ref.
Mn ₂ La ₃ Sb ₃ O ₁₄	7.545	17.798	877.4	[37]
Co ₂ La ₃ Sb ₃ O ₁₄	7.529	17.599	863.9	[36]
Ca ₂ La ₃ Sb ₃ O ₁₄	7.575	18.425	915.6	[39]
Zn ₂ La ₃ Sb ₃ O ₁₄	7.541	17.562	864.9	[38]
Mg ₂ Nb ₃ Sb ₃ O ₁₄	7.502	17.670	861.2	[40]
Ca ₂ La ₃ Nb ₃ O ₁₄	7.652	18.291	928.0	present work

Table 4: List of the different A₂B₃C₃X₁₄ compounds with B = La.

4.2 Rietveld refinement

The structural model published by Fu and Ijdo [39] was considered as the starting model for Ca₂La₃Nb₃O₁₄. A combined Rietveld refinement was carried out with FullProf [35] involving XRD and neutron powder diffraction patterns. The final structural refinement of the appropriate atomic coordinates and temperature factors along with the cell constants, scale factors, zero-points, peak shape parameters and background parameters, converged to the R-factor values gathered in **Table 5**. The complete crystallographic information of Ca₂La₃Nb₃O₁₄ is shown in **Table 6**. The occupation numbers of the mixed sites (Ca/La) for the three possible crystallographic sites 3a, 3b and 9d (**Table 6**) were refined without applying any constraint on the total number of Ca atoms. With the oxidation states of calcium Ca²⁺, lanthanum La³⁺ and niobium Nb⁵⁺, the combined Rietveld refinement enabled to obtain a very small difference of 0.5% in the charge balance with respect to electronic-charge neutrality, yielding the formula Ca_{1.9}La_{3.1}Nb₃O₁₄. The uncertainty of Ca or La contents, calculated using the square-root values of refined occupation numbers, is close to 0.1. Consequently, the final global

formula can be written as $\text{Ca}_2\text{La}_3\text{Nb}_3\text{O}_{14}$. Some selected atomic distances are listed in **Table 7**. The observed, calculated and difference profiles are illustrated in **Figure 5**.

Parameter	X-ray	Neutron
Radiation (Å)	K_{α} Cobalt	1.59445(3)
R_{wp} (%)	11.3	15.3
R_{exp} (%)	7.5	4.5
R_{Bragg} (%)	5.7	7.2
$\text{Ca}_2\text{La}_3\text{Nb}_3\text{O}_{14}$ (weight%)	97.5(9)	97.9(9)
$\text{Ca}_2\text{LaNbO}_6$ (weight%)	2.5(4)	2.1(3)
hkl number	181	252

Table 5: Global results of the combined Rietveld refinement of $\text{Ca}_2\text{La}_3\text{Nb}_3\text{O}_{14}$.

Atom	Position	x	y	z	$B(\text{Å}^2)$	Occ.
Nb	9e	0.5	0.0	0.0	0.76(4)	1
Ca1	3b	0.0	0.0	0.5	0.50(13)	0.65(2)
La1	3b	0.0	0.0	0.5	0.50(13)	0.35(2)
Ca2	3a	0.0	0.0	0.0	1.7(1)†	0.76(2)
La2	3a	0.0	0.0	0.0	1.7(1)†	0.24(2)
Ca3	9d	0.5	0.0	0.5	0.70(4)	0.15(2)
La3	9d	0.5	0.0	0.5	0.70(4)	0.85(2)
O1	6c	0.0	0.0	0.1217(3)	0.38(6)	1
O2	18h	0.4618(2)	0.5382(2)	0.3452(2)	1.11(4)	1
O3	18h	0.4892(2)	0.5108(2)	0.1068(2)	0.99(4)	1
Anisotropic thermal factor ($\times 10^4 \text{Å}^2$)						
Atom	B_{11}	B_{12}	B_{13}	B_{14}	B_{15}	B_{16}
Ca2	87 (17)	87 (17)	15 (2)	43 (8)	0.0	0.0

Table 6: Atomic parameters of $\text{Ca}_2\text{La}_3\text{Nb}_3\text{O}_{14}$ obtained from the combined Rietveld refinement. $a = 7.6525(2)$ (Å), $c = 18.2981(5)$ (Å), space group $R\bar{3}m$ (No.166), $Z = 3$, standard deviations of refined parameters are in parentheses. [† Equivalent atomic displacement parameter (ADP)]

Ca/La	X=Niobium	Occ.	X=Antimony	Occ.
Ca1-O3 ($\times 6$)	2.339(2)	0.65/0.35	2.322(1)	0.94/0.06
Ca2-O1 ($\times 6$)	2.724(4)	0.76/0.24	2.6400(3)	0.60/0.40
Ca2-O3 ($\times 2$)	2.227(4)	0.76/0.24	2.236(7)	0.60/0.40
Ca3-O1 ($\times 2$)	2.357(2)	0.15/0.85	2.340(2)	0.15/0.85
Ca3-O2 ($\times 2$)	2.877(3)	0.15/0.85	2.845(3)	0.15/0.85
Ca3-O3 ($\times 4$)	2.533(2)	0.15/0.85	2.547(1)	0.15/0.85
X-O2 ($\times 4$)	2.016(2)		2.020(1)	
X-O3 ($\times 2$)	1.959(2)		1.931(2)	

Table 7: Interatomic distances (Å) in $\text{Ca}_2\text{La}_3\text{Nb}_3\text{O}_{14}$ and $\text{Ca}_2\text{La}_3\text{Sb}_3\text{O}_{14}$ ^[39] and occupancy ratio of Ca/La.

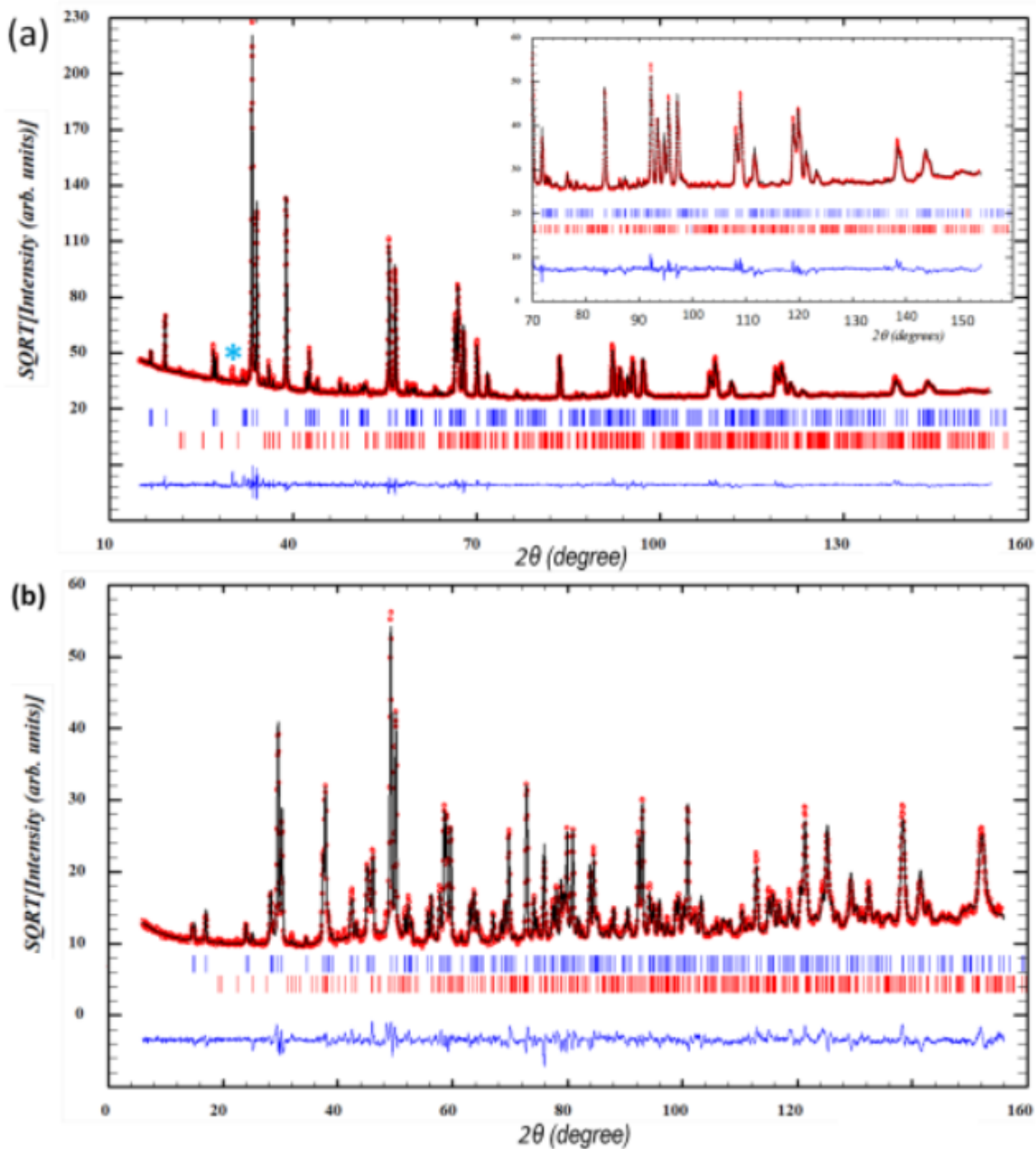


Figure 5: Rietveld refinements on (a) XRD and (b) neutron data at $\lambda = 1.789 \text{ \AA}$ and 1.594 \AA , respectively, in the space group $R\bar{3}m$ for $\text{Ca}_2\text{La}_3\text{Nb}_3\text{O}_{14}$. The red points are the observed data. The solid black and blue lines represent the calculated profile and the difference plot, respectively. The vertical blue and red sticks show the Bragg reflection positions of $\text{Ca}_2\text{La}_3\text{Nb}_3\text{O}_{14}$ and the impurity $\text{Ca}_2\text{LaNbO}_6$, respectively. The weight fractions of the impurity are 2.5(4)% and 2.1(3)% for the refinements on (a) XRD and (b) neutron data, respectively. The blue * in (a) indicates the spectral pollution K_β wavelength position.

4.3 Discussion on the $\text{Ca}_2\text{La}_3\text{Nb}_3\text{O}_{14}$ structure

This recent structural type has been widely described by many authors ^[36][43]. All these compounds are members of the family of Antimony: $\text{A}_2\text{Ln}_3\text{Sb}_3\text{O}_{14}$ with $\text{A} = \text{Mg}, \text{Ca}, \text{Zn}, \text{Mn}, \text{Co}$ and $\text{Ln} = \text{Y}$ or the atoms of the Lanthanide group from La to Dy and Y. The $\text{Ca}_3\text{La}_2\text{Nb}_3\text{O}_{14}$ compound is the first example of this family to adopt this unusual rhombohedral Pyrochlore structure with an atom other than Antimony, namely Niobium. The bond distances in both structures of $\text{Ca}_3\text{La}_2\text{N}_3\text{O}_{14}$ ($\text{N} = \text{Nb}$

or Sb) (**Table 7**) show good similarity. Nb-O and Sb-O distances are in good agreement with the ionic radius of $\text{Nb}^{5+} = 0.64\text{\AA}$ and of $\text{Sb}^{5+} = 0.60\text{\AA}$ in the case of 6-fold coordination.

5. Study of the solid solution of monoclinic $\text{Ca}_{2-x}\text{La}_x\text{Nb}_2\text{O}_{7+\delta}$

During the exploration of the ternary phase diagram, here after, some compositions near the $\text{Ca}_2\text{Nb}_2\text{O}_7$ compound of monoclinic symmetry (**Figure 3**) were synthesized for $x = 0, 0.2, 0.4$ and 1 . The last substitution for $x = 1$ leads to the formula $\text{CaLaNb}_2\text{O}_{7.5}$ with the molar fraction 40% Nb_2O_5 - 40% CaO - 20% La_2O_3 which is referred to as the Y point (**Figure 2**). A solid solution is observed for $x = 0.2$ and $x = 0.4$ (**Table 8** and **Figure 6**).

x	a (Å)	b (Å)	c (Å)	beta (°)	V (Å ³)
0.0	7.687	5.494	13.364	98.34	558.51
0.2	7.725	5.495	13.314	98.43	559.06
0.4	7.734	5.496	13.303	98.46	559.30

Table 8: Cell parameter evolution of monoclinic phase $\text{Ca}_{2-x}\text{La}_x\text{Nb}_2\text{O}_{7+\delta}$.

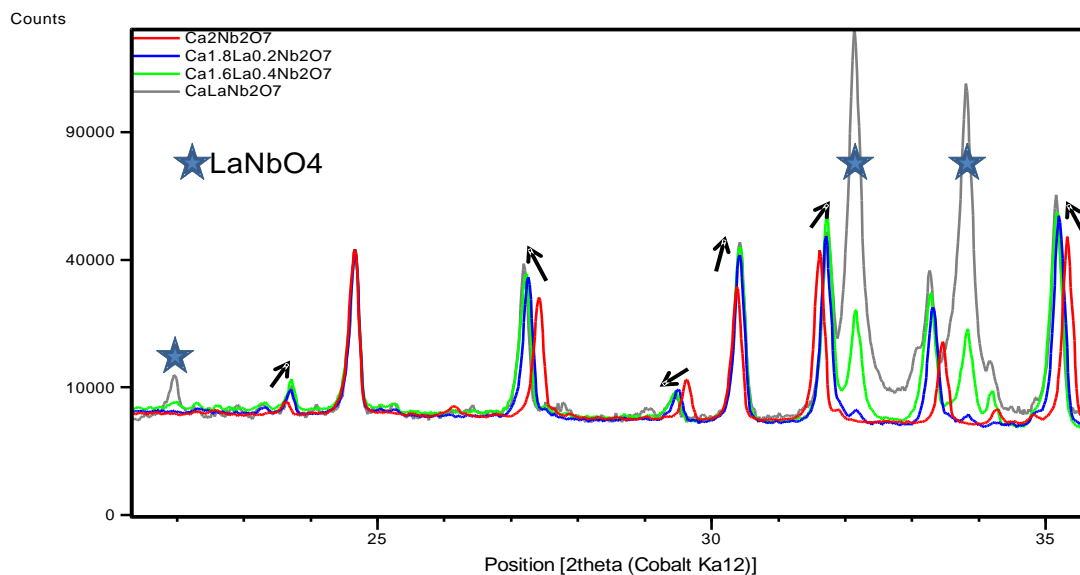


Figure 6: XRD pattern evolution of monoclinic phase $\text{Ca}_{2-x}\text{La}_x\text{Nb}_2\text{O}_{7+\delta}$ ($x = 0; 0.2; 0.4$ and 1). Line shifts are illustrated by the arrows. The stars indicate Fergusonite LaNbO_4 main Bragg peaks.

6. Structural investigation of cubic Pyrochlore $\text{Ca}_8\text{La}_8\text{Nb}_{14.4}\square_{1.6}\text{O}_{56}$

6.1 Rietveld refinement

For some ternary compositions close to the composition of the AC point: 30% Nb_2O_5 - 50% CaO - 20% La_2O_3 (**Figure 2** and **3**), a cubic Pyrochlore structure is observed. The structure of the compound with AC composition having a formula close to $\text{CaLaNb}_2\text{O}_7$ was refined by considering the simple

crystal model based on the cubic Pyrochlore structure of formula $\text{Ca}_2\text{Nb}_2\text{O}_7$ reported by J.T. Lewandowski et al. [42], which crystallizes in the space group $\text{Fd}\bar{3}\text{m}$ (No.227).

A combined Rietveld refinement was carried out with FullProf [35] using XRD and neutron powder diffraction patterns. Our initial structural model involved a mixed site (Ca/La) as well as possible defects at the niobium crystallographic site. The refinement converged to nearly identical values for La and Ca occupation numbers. Consequently, these occupation numbers were fixed to the same value in the final structural refinement leading to a very small difference of 0.4% in the charge balance with respect to electronic-charge neutrality. The R-factor values are gathered in **Table 9** and the complete crystallographic information is shown in **Table 10**. The global formula can then be written as $\text{Ca}_8\text{La}_8\text{Nb}_{14.4}\square_{1.6}\text{O}_{56}$ which indicates the presence of cationic vacancies on the B site ($\text{A}_2\text{B}_2\text{X}_7$).

According to the average volume of oxygen (in the range 18 - 22 \AA^3) observed in oxides, the maximum and minimum number of oxygen atoms per cell are:

$$\text{Maximum number} = 10.6111^3/18 \approx 66$$

$$\text{Minimum number} = 10.6111^3/22 \approx 54$$

From the Rietveld refinement results, a value of 56 oxygen atoms was found which is included in the interval calculated above. This clearly indicated that the number of chemical units per unit cell Z equals 1. The observed, calculated and difference profiles are illustrated in **Figure 7**.

Parameters	X-ray	Neutron
Radiation (\AA)	$\text{K}\alpha$ Cobalt	1.5947(1)
R_{wp} (%)	10.9	11.4
R_{exp} (%)	5.5	3.9
R_{Bragg} (%)	5.8	4.5
$\text{Ca}_8\text{La}_8\text{Nb}_{14.4}\square_{1.6}\text{O}_{56}$ (weight %)	99(1)	99(1)
$\text{Ca}_2\text{LaNbO}_6$ (weight %)	1	1
Number of reflections	56	73

Table 9: Global results for the combined Rietveld refinement of $\text{Ca}_8\text{La}_8\text{Nb}_{14.4}\square_{1.6}\text{O}_{56}$.

Atom	Position	X	y	Z	$B(\text{\AA}^2)$	Occ.
Ca	16d	0.5	0.5	0.5	0.83(3)	0.50
La	16d	0.5	0.5	0.5	0.83(3)	0.50
Nb	16c	0.0	0.0	0.0	0.26(3)	0.906(5)
O ₁	48f	0.3220(1)	1/8	1/8	1.50(2)†	1
O ₂	8b	3/8	3/8	3/8	0.53(4)	1
Anisotropic thermal agitation factor ($\times 10^4 \text{\AA}^2$)						
Atom	B ₁₁	B ₂₂	B ₃₃	B ₁₂	B ₁₃	B ₂₃
O ₁	44(1)	28(1)	28(1)	0.0	0.0	-6(1)

Table 10: Atomic parameters of $\text{Ca}_8\text{La}_8\text{Nb}_{14.4}\square_{1.6}\text{O}_{56}$ obtained from the combined Rietveld refinement.

$a = 10.6111(1)$ (\AA), Space group $\text{Fd}\bar{3}\text{m}$ (No.227), $Z = 1$,

standard deviations of refined parameters are in parentheses. [† Equivalent atomic displacement parameter (ADP)]

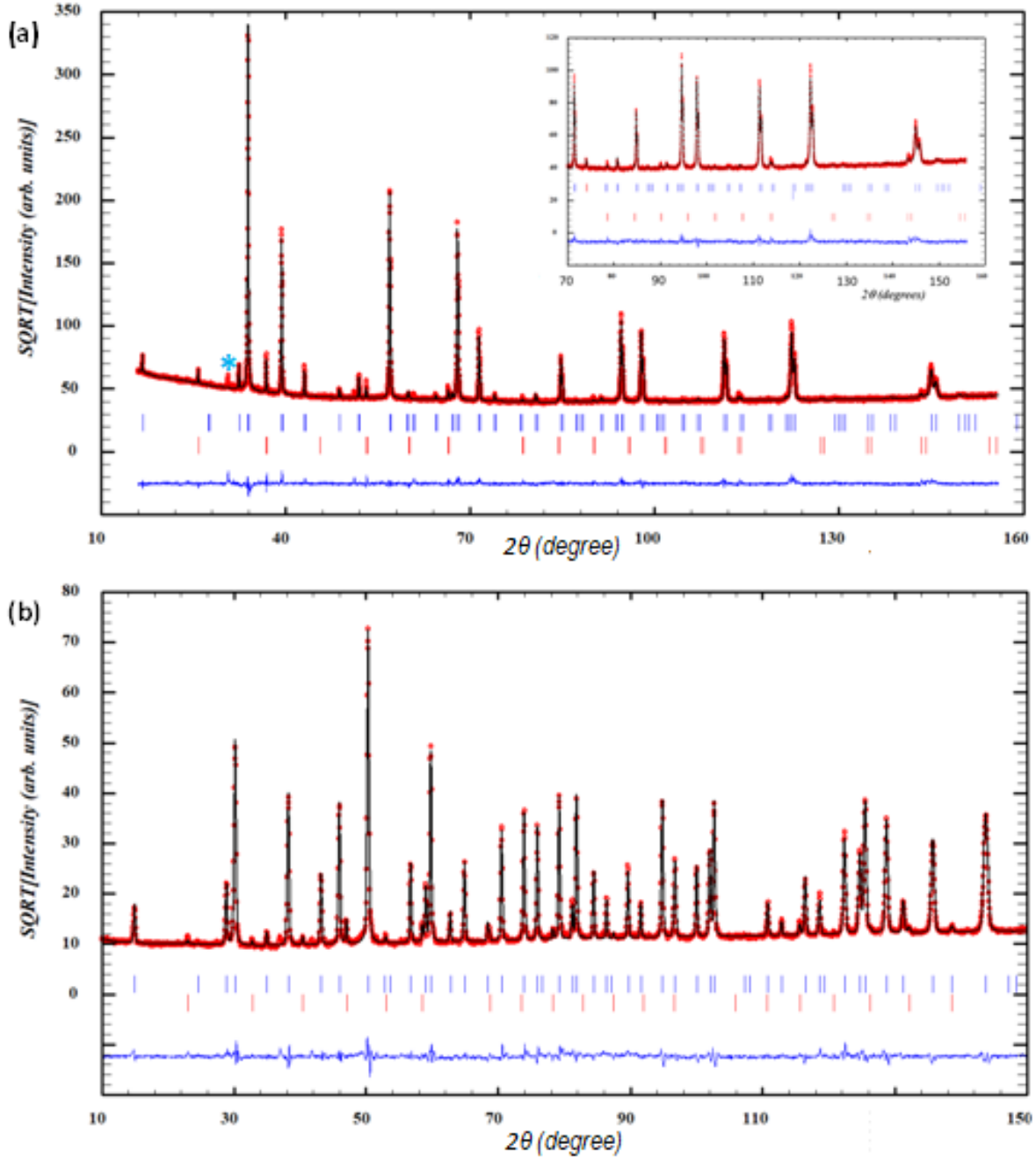


Figure 7: Rietveld refinements on (a) XRD and (b) neutron data at $\lambda = 1.789 \text{ \AA}$ and 1.594 \AA , respectively, in space group $Fd\bar{3}m$ for $\text{Ca}_8\text{La}_8\text{Nb}_{14.4}\square_{1.6}\text{O}_{56}$. The red points are the observed data. The solid black and blue lines represent the calculated profile and the difference plot, respectively. The vertical blue and red sticks show the Bragg reflection positions of $\text{Ca}_8\text{La}_8\text{Nb}_{14.4}\square_{1.6}\text{O}_{56}$ and the impurity $\text{Ca}_2\text{LaNbO}_6$, respectively. The weight fraction of the impurity for both refinements on (a) XRD and (b) neutron data is 1%. The blue * in (a) indicates the spectral pollution K_β wavelength position.

The cubic Pyrochlore $\text{Ca}_2\text{Nb}_2\text{O}_7$ reported by J.T. Lewandowski et al. ^[42] is characterized by a cell parameter $a = 10.445 \text{ \AA}$. The corresponding XRD pattern exhibits a strong (111) peak which is 30% in intensity with respect to the most intense (222) Bragg peak (100%). In case of $\text{Ca}_8\text{La}_8\text{Nb}_{14.4}\square_{1.6}\text{O}_{56}$, the cell parameter is larger ($a = 10.611 \text{ \AA}$) and the intensity of (111) Bragg peak is about 1%. This great difference in intensity for the (111) Bragg peak between $\text{Ca}_2\text{Nb}_2\text{O}_7$ and $\text{Ca}_8\text{La}_8\text{Nb}_{14.4}\square_{1.6}\text{O}_{56}$ is due to

the difference of the atom type at the 16d crystallographic site, which is occupied by Calcium only for the former and by Calcium and Lanthanum in equal proportion for the latter.

7. Impedance and thermal expansion measurements

7.1 Impedance measurement

The Nyquist plots of $\text{Ca}_2\text{La}_3\text{Nb}_3\text{O}_{14}$ and $\text{Ca}_8\text{La}_8\text{Nb}_{14.4}\square_{1.6}\text{O}_{56}$ do not show the Warburg behavior at low frequency. Two behaviors can be observed at high and medium frequencies: one corresponding to the bulk and the other to the boundaries. The total conductivities of the samples were obtained from the equivalent electrical circuit and the fit with ZView^[43]. The Arrhenius plots of the total conductivity, defined as the sum of the grain interior and the grain boundary contributions, in both dry and humid air atmosphere, are displayed in **Figure 8**. The evolutions are nearly linear: the related activation energies are $E_a = 0.59$ eV (dry) and $E_a = 0.46$ eV (wet) for $\text{Ca}_2\text{La}_3\text{Nb}_3\text{O}_{14}$, $E_a = 0.69$ eV (dry) and $E_a = 0.54$ eV (wet) for $\text{Ca}_8\text{La}_8\text{Nb}_{14.4}\square_{1.6}\text{O}_{56}$.

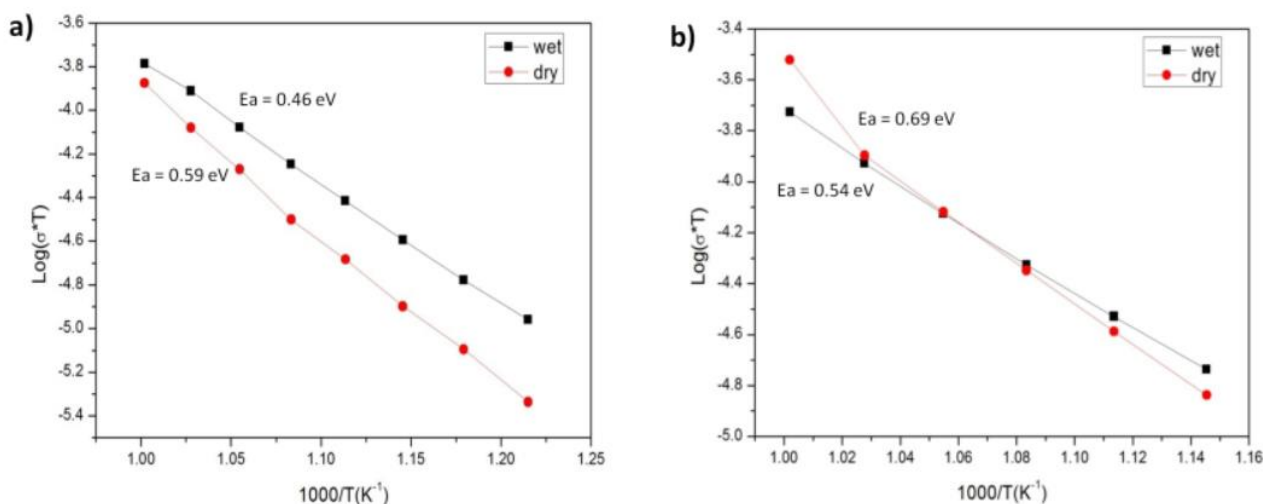


Figure 8: Arrhenius plots of the total conductivity in dry air atmosphere (red) and wet air atmosphere (black) a) for $\text{Ca}_2\text{La}_3\text{Nb}_3\text{O}_{14}$ and b) for $\text{Ca}_8\text{La}_8\text{Nb}_{14.4}\square_{1.6}\text{O}_{56}$, respectively.

7.2 Thermal expansion study

The thermal expansion coefficients of both compounds were determined from high-temperature X-ray diffraction in the temperature range from 40°C to 1000°C using the formula $\alpha = \Delta V / (3 \cdot V_0 \cdot \Delta T)$. The calculated values are $\alpha = 7.25 \times 10^{-6} (\text{K}^{-1})$ and $\alpha = 7.78 \times 10^{-6} (\text{K}^{-1})$ for $\text{Ca}_2\text{La}_3\text{Nb}_3\text{O}_{14}$ and $\text{Ca}_8\text{La}_8\text{Nb}_{14.4}\square_{1.6}\text{O}_{56}$ respectively. These values are lower than that of other materials^[44] as shown in **Table 11**.

The mechanism of oxygen conduction is not that easy to explain. However the materials characterized by low thermal expansion values are frequently modest oxygen ionic conductors [45]. This is verified for both studied compounds.

Material	Thermal expansion coefficient ($\times 10^{-6} \text{ K}^{-1}$)
α -La ₂ Mo ₂ O ₉	14.7
β - La ₂ Mo ₂ O ₉	18.1
La ₁₈ W ₁₀ O ₅₇	14.4
La ₂ WO ₆	11.6
La ₁₀ W ₂ O ₂₁	12.2
La ₇ Nb ₃ W ₄ O ₃₀	11.2
La ₅ NbMo ₂ O ₁₆	10.6

Table 11: Thermal expansion coefficient α of some materials in the La-Mo/W-O compounds.

8. Re-investigation of the center of ternary diagram La₂O₃-Nb₂O₅-CaO

Rietveld refinements on XRD data were performed for all investigated compositions points (supplementary information). The detailed analysis of the refinements revealed 8 different composition zones, labeled 1 to 8, as shown in **Figure 3**. The corresponding phases and their weight percentage are summarized in **Table 12** and **13**.

Zone	Sample	Phase and percentage of weight (%)					
		Phase	Weight (%)	Phase			
1	K R	La ₃ NbO ₇	31.4	LaNbO ₄	18.1	Ca ₂ La ₃ Nb ₃ O ₁₄	50.5
			8.6		9.2		82.2
2	AB WXAB WR RWX	La ₃ NbO ₇	37.4	Ca ₂ LaNbO ₆	48.1	Ca ₂ La ₃ Nb ₃ O ₁₄	14.5
			21.1		25.3		53.6
			25.6		10.8		63.6
			1.9		2.4		95.7
3	ACAF	Ca ₂ Nb ₂ O ₇ cubic	41.4	Ca ₂ LaNbO ₆	29.7	Ca ₂ La ₃ Nb ₃ O ₁₄	28.9
4	XS	LaNbO ₄	29.2	Ca ₂ Nb ₂ O ₇ cubic	57.3	Ca ₂ La ₃ Nb ₃ O ₁₄	13.5
5	S	LaNbO ₄	66.1	Ca ₂ Nb ₂ O ₇ mono	20.1	Ca ₂ Nb ₂ O ₇ cubic	13.8
6	AI	Ca ₂ Nb ₂ O ₇ cubic	14.0	Ca ₂ LaNbO ₆	84.8	Ca ₄ Nb ₂ O ₉	1.1
7	AG	Ca ₂ La ₂ O ₇ cubic	30.2	Ca ₂ La ₂ O ₇ mono	47.3	Ca ₄ Nb ₂ O ₉	22.5
8	MST AD	LaNbO ₄	64.2	Ca ₂ Nb ₂ O ₇ mono	27.5	CaNb ₂ O ₆	8.3
			13.6		68.5		17.9

Table 12: Identified phases and their weight fractions of synthesized samples in the different zones.

Line between two zones	Sample	Phase and percentage of weight (%)		
1-2	KQR	La ₃ NbO ₇ 30.5	Ca ₂ La ₃ Nb ₃ O ₁₄ 69.5	
2-unsolved zone	Q	La ₃ NbO ₇ 74.3	Ca ₂ LaNbO ₆ 25.7	
2-3	XABAC ABAC	Ca ₂ LaNbO ₆ 80.1 18.5	Ca ₂ La ₃ Nb ₃ O ₁₄ 14.4 55.7	Ca ₂ Nb ₂ O ₇ cubic * 5.5 25.8
1-4	RSX	LaNbO ₄ 19.7	Ca ₂ La ₃ Nb ₃ O ₁₄ 80.3	
3-4	ACX	Ca ₂ La ₂ O ₇ cubic 70.8	Ca ₂ La ₃ Nb ₃ O ₁₄ 29.2	
4-5	LS SXY XYAC	LaNbO ₄ 59.4 43.0 15.9	Ca ₂ La ₂ O ₇ cubic 40.6 57.0 84.1	
6-7	ACAFAG	Ca ₂ La ₂ O ₇ cubic 72.1	Ca ₄ Nb ₂ O ₉ 27.9	
5-8	Y SY YACAD	LaNbO ₄ 44.1 50.4 33.2	Ca ₂ Nb ₂ O ₇ mono 55.9 49.6 66.8	
8-unsolved zone	T M	LaNbO ₄ 45.1 69.7	CaNb ₂ O ₆ 54.9 30.3	

Table 13: Identified phases and their weight fractions of synthesized samples on the boundary lines between two zones.
* means that the number of observed phases is not in agreement with Gibbs rules.

9. Conclusion

The structures of the two newly identified compounds $\text{Ca}_2\text{La}_3\text{Nb}_3\text{O}_{14}$ and $\text{Ca}_8\text{La}_8\text{Nb}_{14.4}\square_{1.6}\text{O}_{56}$ were determined. The synthesis of the almost pure compound $\text{Ca}_2\text{La}_3\text{Nb}_3\text{O}_{14}$ requires a very long thermal process at high temperature (1300°C - 1400°C, during more than 12 days). This slow kinetic process makes it very difficult to synthesize pure phase with the nominal composition.

The structure of $\text{Ca}_2\text{La}_3\text{Nb}_3\text{O}_{14}$ was determined by using microscopy electron diffraction, X-ray and neutron powder diffraction data. This compound crystallizes in the space group $R\bar{3}m$ (No.166) ($Z = 3$) with the cell parameters $a = 7.6525(2)$ (Å) and $c = 18.2981(5)$ (Å). This niobium compound is the first example of structure which adopts the unusual rhombohedral Pyrochlore structure $\text{A}_2\text{Ln}_3\text{Sb}_3\text{O}_{14}$ with $A = \text{Mg, Ca, Zn, Mn, Co}$ and Ln the Lanthanide group from La to Dy and Y.

The structure of $\text{Ca}_8\text{La}_8\text{Nb}_{14.4}\square_{1.6}\text{O}_{56}$, derived from the cubic Pyrochlore $\text{Ca}_{2-x}\text{La}_x\text{Nb}_2\text{O}_{7+\delta}$, was refined by using X-ray combined with neutron powder diffraction data. In this compound, which crystallizes in the cubic space group $\text{Fd}\bar{3}m$ (No.227) ($Z = 1$) with the cell parameter $a = 10.6111(1)$ (Å), Calcium and Lanthanum atoms are randomly distributed on the same crystallographic site 16d with the occupancy ratio of 0.5/0.5.

Regarding transport property, both compounds display a modest ionic conductivity in both dry and humid air atmosphere.

A solid solution was observed for cubic Pyrochlore $\text{Ca}_{2-x}\text{La}_x\text{Nb}_2\text{O}_{7+\delta}$ as well as monoclinic Pyrochlore $\text{Ca}_{2-x}\text{La}_x\text{Nb}_2\text{O}_{7+\delta}$ in the range from $x = 0$ to $x = 0.4$.

The central region of the ternary diagram $\text{La}_2\text{O}_3 - \text{Nb}_2\text{O}_5 - \text{CaO}$ was investigated: Rietveld refinements on XRD data were performed for all investigated composition points. The detailed analysis of the refinements revealed that the central region is composed of 8 zones which are all in agreement with Gibbs rules in the thermodynamic field.

Credit author statement

Qiong YE: Synthesis, Analysis, Investigation, Software, Data curation, Writing - original draft.

Alain JOUANNEAUX: Validation, Analysis, Investigation, Software, Data curation.

Emmanuelle SUARD: Neutron data collection.

François GOUTENOIRE: Validation, Analysis, Software, Data curation, Writing - original draft, Supervision.

All authors contributed to this manuscript.

Declaration of competing interest

The authors declare that they have no known competing financial interests or personal relationships that could have appeared to influence the work reported in this paper.

Bibliography

- [1] S. Srinivasan, R. Mosdale, P. Stevens, C. Yang, Fuel cells: reaching the era of clean and efficient power generation in the twenty first century, *Annu. Rev. Energy Environ*, **24**(1999)281-328.
- [2] W. H. J. Graus, M. Voogt, E. Worrell, International comparison of energy efficiency of fossil power generation, *Energy Policy*, **35**(2007)3936-3951.
- [3] F. J. Rohr, High-temperature fuel cells in solid electrolytes, general principles, characterization, materials, applications, edited by P. Hagemuller and W. Vangool, (Academic press, New York,1978) p.431.
- [4] J. F. Baumard, P. Abelard, Defect structure and transport properties of ZrO₂-based solid electrolytes in science and technology of zirconia II, edited by A. H. Hever, N. Claussen, M. Ruble, American ceramic society, Columbus, OH(USA), (1983) p.555.
- [5] V. V. Kharton, F. M. B. Marques, A. Atkinson, Transport properties oxide electrolyte ceramics : a brief review, *Solid State Ionics*, **174**(2004)135-149.
- [6] M. Biswas, K. C. Sadanala, Electrolyte materials for solid oxide fuel cell, *Powder Metallurgy & Mining*, **2**(2013)2-4.
- [7] N. M. Sammes, Z. Cai, Ionic conductivity of ceria/yttria stabilized zirconia electrolyte materials, *Solid State Ionics*, **100**(1997)39-44.
- [8] T. Takahashi, H. Iwahara, Ionic conduction in perovskite-type oxide solid solution and its application to the solid electrolyte fuel cell, *Energy Conversion*, **11**(1971)105-111.
- [9] S. C. Singhal, K. Kendall, High-temperature solid oxide fuel cells: fundamentals, design and applications, Elsevier Science, (2003).
- [10] K. R. Kendall, C. Navas, J. K. Thomas, H. C. Z. Loye, Recent developments in perovskite-based oxide ion conductors, *Solid State Ionics*, **82**(1995)215-223.
- [11] P. Lacorre, F. Goutenoire, O. Bohnke, R. Retoux, Y. Laligant, Designing fast oxide-ion conductors based on La₂Mo₂O₉, *Nature*, **404**(2000)856-858.
- [12] F. Goutenoire, O. Isnard, R. Retoux, P. Lacorre, Crystal structure of La₂Mo₂O₉, a new fast oxide-ion conductor, *Chem. Mater.*, **12**(2000)2575.
- [13] F. Goutenoire, O. Isnard, R. Retoux, O. Bohnke, Y. Laligant, P. Lacorre, Structural and transport characteristics of the LAMOX family of fast oxide-ion conductors, based on lanthanum molybdenum oxide La₂Mo₂O₉, *J. Mater. Chem.*, **11**(2001)119.
- [14] N. Q. Minh, Ceramic fuel cells, *J. Am. Ceram. Soc.*, **76**(1993)563-88.
- [15] A. Kahn-Harari, L. Mazerolles, D. Michel, F. Robert, Structural description of La₃NbO₇, *Journal of Solid State Chemistry*, **116**(1995)103-106.
- [16] L. Cai, J. C. Nino, Synchrotron and neutron powder diffraction study of phase transition in weberite-type Nd₃NbO₇ and La₃NbO₇, *Journal of Solid State Chemistry*, **184**(2011)2263-2271.
- [17] A. Chesnaud, M. D. Braida, S. Estradé, F. Peiro, A. Tarancon, A. Morata, G. Dezanneau, High-temperature anion and proton conduction in RE₃NbO₇ (RE = La, Gd, Y, Yb, Lu) compounds, *Journal of the European Ceramic Society*, **35**(2015)3051-3061.
- [18] K. Kato, K. Toyoura, A. Nakamura, K. Matsunaga, First-principles analysis on proton diffusivity in La₃NbO₇, *Solid State Ionics*, **262**(2014)472-475.
- [19] K. Kato, K. toyoura, A. Nakamura, K. Matsunaga, Proton channels along oxygen octahedral chains in La₃NbO₇, *J. phys. Chem. C*, **118**(2014)9377-9384.

- [20] R. Haugrud, T. Risberg, Protons in acceptor-doped La_3NbO_7 and La_3TaO_7 , *Journal of the Electrochemical Society*, **156**(2009)B425-B428.
- [21] B. J. Kennedy, C. J. Howard, Y. Kubota, K. Kato, Phase transition behaviour in the A-site deficient perovskite oxide $\text{La}_{1/3}\text{NbO}_3$, *Journal of Solid State Chemistry*, **177**(2004)4552-4556.
- [22] A. M. George, A. N. Virkar, Mixed iono-electronic conduction in $\beta\text{-LaNb}_3\text{O}_9$, *J. Phys. Chem. Solids*, **49**(1988)743-751.
- [23] S. W. Arulnesan, P. Kayser, J. A. Kimpton, B. J. Kennedy, Studies of the fergusonite to scheelite phase transition in LnNbO_4 orthoniobates, *Journal of Solid State Chemistry*, **277**(2019)229-239.
- [24] R. Haugrud, T. Norby, High-temperature proton conductivity in acceptor-doped LaNbO_4 , *Solid State Ionics*, **177**(2006)1129-1135.
- [25] L. Bi, E. Fabbri, E. Traversa, Solid oxide fuel cells with proton-conducting $\text{La}_{0.99}\text{Ca}_{0.01}\text{NbO}_4$ electrolyte, *Electrochimica Acta*, **260**(2018)748-754.
- [26] G. C. Mather, C. A. J. Fisher, M. S. Islam, Defects, dopants, and protons in LaNbO_4 , *Chem. Mater.*, **22**(2010)5912-5917.
- [27] T. Norby, A. Magraso, On the development of proton ceramic fuel cells based on Ca-doped LaNbO_4 as electrolyte, *Journal of power sources*, **282**(2015)28-33.
- [28] A. M. Frolov, A. A. Evdokimov, The isothermal section of $\text{CaO-La}_2\text{O}_3\text{-Nb}_2\text{O}_5$ system. *Russ J. Inorg Chem.(English Translation)*, **32**(1987)1771-3.
- [29] I. C. Madsen and R. J. Hill, Collection and analysis of powder diffraction data with near constant counting statistics, *Journal of Applied Crystallography*, **27**(1994)385-392.
- [30] P. E. Werner, Trial-and-error computer methods for the indexing of unknown powder patterns, *Zeitschrift fur Kristallographie*, **120**(1964)375-387.
- [31] T. Degen, M. Sadki, E. Bron, U. König, G. Nenert, The HighScore suite. *Powder Diffr.*, **29**(2014)13-18.
- [32] P. M. de Wolf, A simplified criterion for the reliability of a powder pattern indexing, *Journal of Applied Crystallography*, **1**(1968)108-113.
- [33] M. Klinger, A. Jäger. Crystallographic Tool Box (CrysTBox): automated tools for transmission electron microscopists and crystallographers. *Journal of Applied Crystallography*, **48**(2015), doi:10.1107/S1600576715017252.
- [34] A. Le Bail, H. Duroy, J.F. Fourquet, Ab Initio Structure Determination of LiSbWO_6 by X-ray powder diffraction, *Mat. Res. Bull.*, **23**(1988)447-452.
- [35] J. Rodriguez-Carvajal, FullProf Suite Program.
- [36] K. Li, Y. Hu, Y. Wang, T. Kamiyama, B. Wang, Z. Li, J. Lin, Syntheses and properties of a family of new compounds $\text{RE}_3\text{Sb}_3\text{Co}_2\text{O}_{14}$ (RE=La, Pr, Nd, Sm-Ho) with an ordered pyrochlore structure, *Journal of Solid State Chemistry*, **217**(2014)80-86.
- [37] W. T. Fu, D. J. W. Ijdo, Crystal structure of $\text{Mn}_2\text{Ln}_3\text{Sb}_3\text{O}_{14}$ (Ln=La, Pr and Nd): A new ordered rhombohedral pyrochlore, *Journal of Solid State Chemistry*, **213**(2014)165-168.
- [38] M. B. Sanders, K. M. Baroudi, J. W. Krizan, O. A. Mukadam, R. J. Cava, Synthesis, crystal structure, and magnetic properties of novel 2D kagome materials $\text{RE}_3\text{Sb}_3\text{Mg}_2\text{O}_{14}$ (RE=La, Pr, Sm, Eu, Tb, Ho): Comparison to $\text{RE}_3\text{Sb}_3\text{Zn}_2\text{O}_{14}$ family, *Phys. Status Solidi B*, **253**(2016)2056-2065, doi:10.1002/pssb.201600256.
- [39] W.T. Fu, D. J. W. Ijdo, New rhombohedral pyrochlores $\text{Ca}_2\text{Ln}_3\text{Sb}_3\text{O}_{14}$ (Ln lanthanide and Y): space group revised, *Journal of Solid State Chemistry*, **229**(2015)330-335.
- [40] A. Scheie, M. Sanders, J. Krizan, Y. Qiu, R. J. Cava, and C. Broholm, Effective spin-1/2 scalar chiral order on kagome lattices in $\text{Nd}_3\text{Sb}_3\text{Mg}_2\text{O}_{14}$, *Phys. Rev. B*, **93**(2016)180407, doi:10.1103/PhysRevB.93.180407.
- [41] F. Piccinelli, I. Carrasco, C. G. Ma, A. M. Srivastava, M. Bettinelli, Disorder-induced breaking of the local inversion symmetry in rhombohedral pyrochlores $\text{M}_2\text{La}_3\text{Sb}_3\text{O}_{14}$ (M =

- Mg or Ca): a structural and spectroscopic investigation, *Inorg. Chem.*, **57**(2018)9241-9250.
- [42] J. T. Lewandowski, I. J. Pickering, A. J. Jacobson, Hydrothermal synthesis of calcium-niobium and tantalum oxides with pyrochlore structure, *Materials Research Bulletin*, **27**(1992)981-988.
- [43] D. Jacobson, ZView, version 3.5h; Scribner Associates, Inc: Southern Pines, NC, ©Copy - right 1996-2019.
- [44] T. D. Vu, F. Krischen, M. Barre, K. Adil, A. Jouanneaux, E. Suard, F. Goutenoire, Crystal structure and ion conducting properties of $\text{La}_5\text{NbMo}_2\text{O}_{16}$, *Journal of Solid State Chemistry*, **237**(2016)411-416.
- [45] S. Taniguchi, M. Aniya M, Relationship between thermal expansion, ionic conduction and ionicity in perovskite-type oxides, *Int. Conf. Physics of Solid State Ionics(ICPSSI-3)*, *J. Phys. Soc. Jpn.*, **79**(2010)106-108.